Mie-Resonant Structural Color of Silicon Nanosphere Monolayer Coupled with Fabry-Pérot Cavity

Song, Jialu
Tanaka, Haruki
Moriasa, Keisuke
Sugimoto, Hiroshi
Fujii, Minoru

(Citation)
ACS Applied Optical Materials,2(7):1420-1426

(Issue Date)
2024-07-26

(Resource Type)
journal article

(Version)
Accepted Manuscript

Mie-Resonant Structural Color of Silicon Nanosphere Monolayer Coupled with Fabry–Pérot Cavity

Jialu Song, Haruki Tanaka, Keisuke Moriasa, Hiroshi Sugimoto, Minoru Fujii*

Department of Electrical and Electronic Engineering, Graduate School of Engineering, Kobe University, 1-1 Rokkodai, Nada, Kobe 657-8501, Japan

*e-mail: sugimoto@eedept.kobe-u.ac.jp

KEYWORDS: Mie resonance, structural color, silicon nanoparticles, Fabry–Pérot interference, mode coupling

Abstract

Silicon (Si) nanospheres (NSs) 100-200 nm in diameter exhibit size-dependent scattering colors due to the Mie resonances. Because of the very high scattering efficiency, reflectance of ~50 % can be achieved in the monolayers, and thus ultra-thin and -lightweight color painting is possible with the Si NSs. In this work, we explore the possibility of controlling the color of Si NS monolayers by coupling with a Fabry–Pérot cavity for potential applications in dynamic color displays and environment sensors. First, scattering spectra of a single Si NS placed on a Si mirror via a silicon dioxide (SiO_2) spacer are studied by numerical simulations for different spacer thicknesses. Similar simulations are then made for Si NS monolayers. The numerical results reveal

that the reflected color can be tuned through the coupling strength of the spacer playing as a Fabry-Perot cavity and Mie resonances of Si NSs. Following the numerical results, Si NS monolayers are produced from the colloidal suspensions by the Langmuir-Blodgett method on surface-oxidized Si wafers, and the color control is experimentally demonstrated.

1. Introduction

Structural colors are those produced by interference, diffraction, scattering and absorption of micro- or nano-objects that can be found in nature such as feathers and butterflies.[1,2] Compared to conventional color pigments and dyes, structural colors do not fade and have long-term stability as long as the structure is sustained. In early history, the structural color has been achieved artificially by interference or diffraction of light in a periodic structure of subwavelength-size components. Recently, structural color devices employing designed nanostructures composed of optical nanoantennas with diverse working principles have been developed thanks to the advancement of nanofabrication technology.[3–8]

Among different working principles for structural coloration, Mie scattering of high–refractive index dielectric nanostructures has several advantages such as a non-iridescent coloration, easy control of the scattering color by geometrical parameters,[4,9–14] and wide color gamut.[9,15–17] Silicon (Si) is the most widely used high refractive index (n = ~4) materials for structural coloration because of the low extinction coefficient and the established nanofabrication technology.[10,18–27] Furthermore, colloidal suspension of almost mono-dispersed Si nanospheres (Si NSs) has been developed and structural coloration in a large area by painting has been achieved.[18,28] Because of

the large scattering efficiency of a Si NS, the peak reflectance can reach ~50 % even in the monolayer film, suggesting possible very thin and very light (<0.5 g/m^2) structural coloration.

In general, a structural color is fixed once the structure is formed. If a structural color can be controlled by external stimuli, it paves the way for applications in different fields such as dynamic color displays and environment sensors. Therefore, there has been a great deal of research on controlling structural colors. For example, reflection colors of Mie resonators are changed by electric field,[29–31] mechanical stress,[31–33] humidity,[34–36] etc. In many cases, the strategy to change color is using coupling with other optical modes and modifying the coupling strength.[37–39] In this work, we study the coupling of Mie modes of a Si NS monolayer and a Fabry–Pérot cavity mode and investigate how the reflection color is modified by the cavity length.

In this work, we fabricate monolayers of different sizes Si NSs on a Si mirror via a silicon dioxide (SiO_2) spacer, which acts as a Fabry–Pérot cavity, and study the coupling properties theoretically and experimentally. We first study how Mie scattering of a single Si NS is modified by the Fabry–Pérot mode by numerical simulations. We then study the reflection properties of 2D hexagonal arrays of Si NSs placed on the cavity for different NS diameters and cavity lengths. Finally, we produce Si NS monolayers from the colloidal suspensions by the Langmuir-Blodgett method on surface-oxidized Si wafers and study the specular and diffuse reflectance spectra. We show that the reflection peak wavelength can be shifted at most 100 nm by changing the cavity length which can be manifested as a reflection color change.

2. Results and Discussion

2.1. Simulation study on coupling of Mie mode of Si NS monolayer and Fabry–Pérot mode

Figure 1a shows the calculated backward scattering spectrum (NA of detection: 0.8) of a Si NS 160 nm in diameter in vacuum, and the scattering color calculated from the spectrum. Scattering by the electric dipole (ED) mode at ~525 nm and the magnetic dipole (MD) mode at ~630 nm results in the yellow scattering color. We first calculate how the scattering property of the single Si NS is modified by coupling with a Fabry–Pérot mode. The calculation model is schematically shown in Figure 1b. A Si NS is placed on a SiO_2 film formed on Si surface (SiO_2/Si substrate). Incident light (k_i) comes from the normal to the surface and scattered light is assumed to be detected by an objective lens of NA=0.8. In the figure, the electric field ($|\boldsymbol{E}|^2$) and magnetic field ($|\boldsymbol{H}|^2$) intensities of the standing wave by the reflection from a bottom Si mirror are schematically shown. Since reflection at the air/SiO_2 interface is very small, it does not strongly modify the standing wave. Therefore, the structure can be modeled as a Si NS occupying different longitudinal positions in the standing wave depending on the SiO_2 thickness (t_s). Figure 1c shows a contour plot of the scattering spectra. The vertical axis is the SiO_2 thickness (0 to 250 nm). The figure reveals that the resonance wavelengths of the ED and MD modes are almost not affected by the SiO_2 thickness, and only the intensities are modulated. Figure 1d-f shows calculated scattering spectra for t_s = 200, 165, and 35 nm, respectively, extracted from Figure 1c. We can see that the relative intensity of the ED and MD modes is strongly modified by the SiO_2 thickness; at t_s = 35 nm, the ED mode dominates the spectrum, while at t_s = 165 nm the MD mode dominates. This is due to π phase difference between the electric and magnetic field intensities in the standing wave; the ED scattering becomes strong at t_s of the electric field maxima, while the MD scattering at t_s of the magnetic field maxima. The modulation of the relative intensity appears as a significant change of the scattering color as can be seen in the insets in Figure 1d-f.

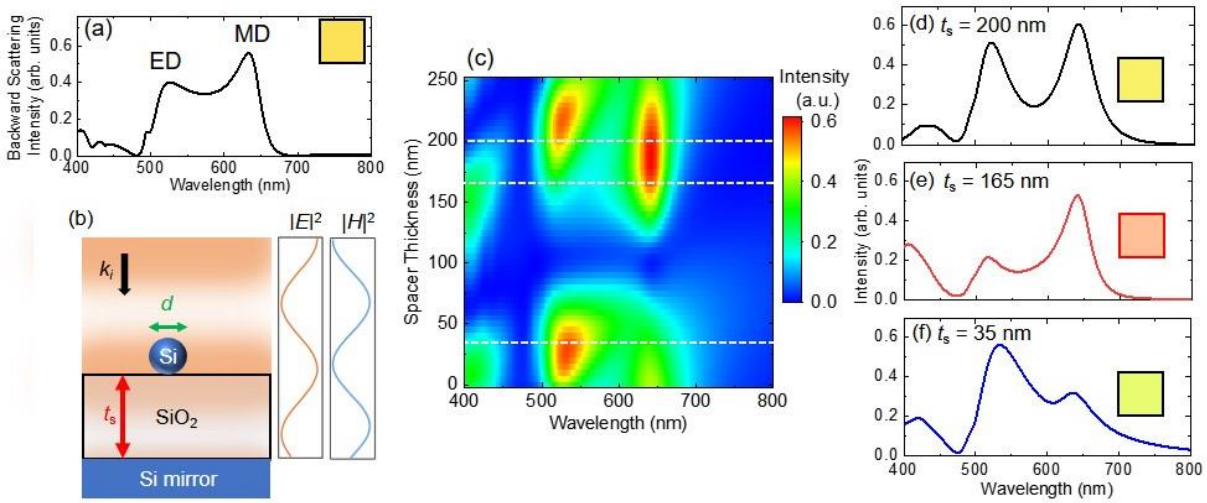

Figure 1. (a) Calculated backward scattering spectrum (NA of detection: 0.8) of a single Si NS 160 nm in diameter in vacuum, and the scattering color calculated from the spectrum. (b) Schematic of the model structure for calculation of scattering spectra of a Si NS placed on a SiO_2 film (thickness: t_s) grown on a Si wafer. The incident light (k_i) is normal to the surface. Electric ($|E|^2$) and magnetic field ($|H|^2$) intensities of the standing wave are also schematically shown. (c) Contour plot of calculated backward scattering spectra (NA of detection: 0.8) of a Si NS 160 nm in diameter on a SiO_2 film grown on a Si wafer. The vertical axis is the SiO_2 thickness (0 to 250 nm). (d-f) Calculated scattering spectra of a Si NS 160 nm in diameter on a SiO_2 film grown on a Si wafer. The SiO_2 thickness is (d) 200, (e) 165 and (f) 35 nm. Insets are scattering colors calculated from the spectra.

Figure 2a shows the calculated reflectance spectrum of a hexagonal array of Si NSs in air. The diameter of a Si NS (d) and the gap between them (g) are 160 nm and 20 nm, respectively. In contrast to the double-peak scattering spectrum of a single Si NS in Figure 1a, the NS monolayer has a single reflectance peak at ~550 nm. In order to study the mechanism of the spectral change, we calculated the scattering spectra of a Si NS and a NS monolayer in air and extracted the

contributions of different Mie modes by the multipole decomposition.[40] The results are shown in Supporting Information (Figure S1). In a monolayer, the ED and MD modes are significantly broadened and their overlap increases. The amplitudes of the two modes are almost equal at ~550 nm. This results in the reflectance maximum at 550 nm due to the Kerker effect.[12] The overlap of the two modes decreases with increasing g, and distinctive MD and ED peaks appear in the reflectance spectra when g = ~100 nm.[28]

We then calculate the reflectance spectra of a Si NS monolayer on a SiO_2/Si substrate. Figure 2b shows the cross-sectional view of a model structure for calculation; a hexagonal array of 160 nm-diameter Si NSs is placed on a SiO_2/Si substrate. The NS-to-NS gap is assumed to be 20 nm and the SiO_2 film thickness is changed from 0 to 250 nm. Note that the gap length does not strongly affect the reflectance spectra in a small gap range (see Figure S4 in Supporting Information). Figure 2c shows the contour plot of the calculated reflectance spectra. The reflectance peak shifts slightly to longer wavelength with increasing t_s, and the intensity is strongly modulated due to the coupling with the Fabry–Pérot cavity formed between the Si NS monolayer and the Si mirror. Figure 2c-e shows the reflectance spectra at t_s= 220, 170 and 120 nm, respectively, extracted from Figure 2b. At t_s = 120 nm, a broad peak appears at 500-650 nm. It splits into two peaks at t_s = 170 nm. This is due to the existence of a valley of the Fabry–Pérot interference at the dip wavelength. Further increase of the spacer thickness to 220 nm shifts the dip to ~600 nm, resulting in the appearance of a dominant peak at 540 nm. This makes the reflection color greenish. By comparing Figure 1d-f and Figure 2c-e, we notice that the color changes more prominently by the spacer thickness in a Si NS monolayer than in a single Si NS. This is due to the shift of the Fabry–Pérot dip within the Mie-resonant reflectance band with increasing t_s. This effect is not prominent in a single Si NS because of the small refractive index contrast at the upper boundary.

In Mie resonance of a Si NS, the most important parameter to control the scattering color is the size. We therefore calculate spacer thickness dependence of the reflection spectra for different diameter Si NSs. The calculated reflectance spectra are shown in Supporting Information (Figure S2), and the colors calculated from the spectra are summarized in Figure 2f. In the figure, the diameter is changed from 115 to 180 nm, and the spacer thicknesses are changed from 0 to 200 nm. The gap between Si NSs is fixed at 20 nm. We can see that by controlling both the SiO_2 film thickness and the Si NS diameter, the color can be controlled in a wide range.

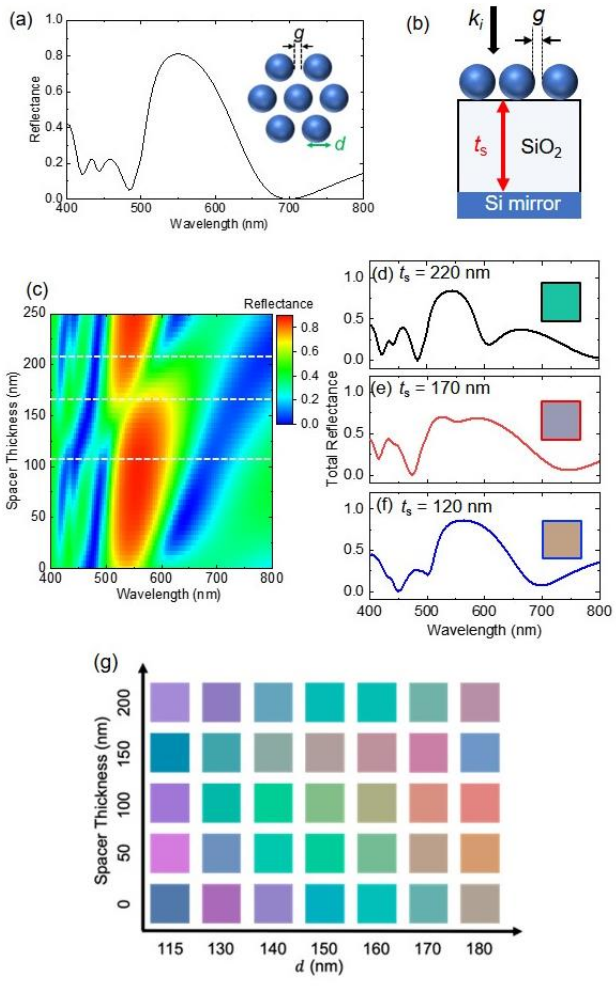

Figure 2. (a) Reflectance spectrum of a hexagonal array of a Si NS monolayer in air. Inset: schematic of a Si NS monolayer (top-view). The diameter of Si NSs is 160 nm and the gap between the NSs is 20 nm. (b) Schematic of a hexagonal array of a Si NS monolayer on a SiO_2/Si substrate (cross-sectional view). The incident light (k_i) is normal to the surface. (c) Reflectance spectra of Si NS monolayers made from 160 nm-diameter Si NSs. The vertical axis is the SiO_2 spacer thickness (t_s = 0 to 250 nm). (d-f) Reflectance spectra of Si NS monolayers at t_s = (d) 220, (e) 170 and (f) 120 nm extracted from (c). Insets are reflection colors calculated from the spectra. (g) Predicted colors calculated from reflectance spectra of Si NS monolayers. The abscissa is the diameter (d = 115 to 180 nm), and the ordinate is the SiO_2 spacer thickness (t_s = 0 to 200 nm).

2.2. Fabrication of Si NS monolayer coupled with Fabry–Pérot cavity and the reflection property

Si NSs are produced by thermal disproportionation reaction of Si monoxide (SiO) powder. Details of the preparation procedure are shown in the experimental section. Figure 3a shows a transmission electron microscope (TEM) image of the Si NSs, and a photograph of the colloidal suspension that contains different sizes Si NSs.[28,41,42] The NSs are nearly perfectly spherical. Figure 3b shows the high-resolution TEM image. The lattice fringe corresponds to the {111} plane of Si crystal can be seen. Figure 3c shows a Raman scattering spectrum of a single Si NS together with that of a crystalline Si wafer. The sharp peak at 520 cm^{-1} with the line width comparable to that of a Si wafer evidences the high crystallinity. Figure 3d shows the dark-field scattering spectrum (red curves) of a Si NS with the diameter of 156 nm placed on a SiO_2 substrate together with the calculated scattering spectrum (gray dashed curve). The good agreement between experimental and calculated spectra again confirms the high quality of the NS.

Figure 3e shows The NSs in the suspension are separated by size by a density gradient centrifugation process.[21,22,42] Figure 3b shows photos after the size separation process. Clear Mie scattering color can be seen. Below the photos, the average diameter (d_{ave}) and the coefficients of variation of the size distribution (C_v) defined by the standard deviation divided by d_{ave} are shown. Figure 3c shows the extinction spectra of the colloidal suspensions. The Mie scattering peaks can be clearly seen.

Monolayers of Si NSs are fabricated from colloidal suspensions. First, a Si wafer is cut into 1.7 cm x 1 cm and oxidized in air at 1100°C. The oxide thickness is changed from 20 to 200 nm by the oxidation duration (see Supporting Information (Figure S3)). On the SiO_2/Si substrates, Si NS monolayers are formed by the Langmuir-Blodgett (LB) method.[28] Figure 3d shows an SEM image of a Si NS monolayer. A densely packed 2D layer of Si NSs is formed, although a few NSs are overlapped on the layer.

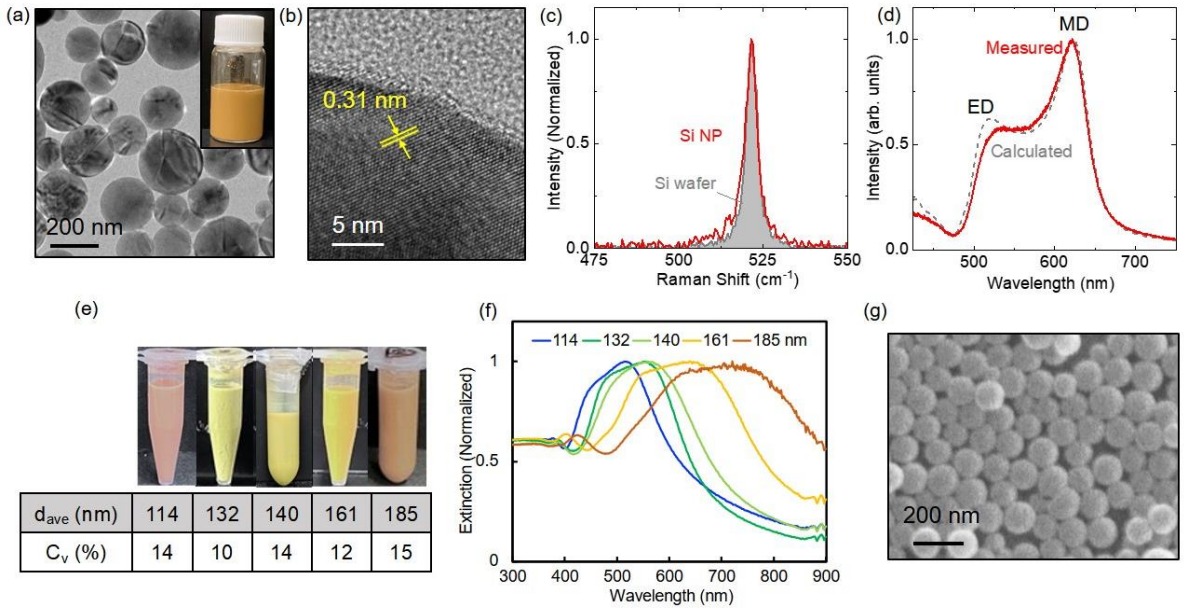

d_{ave} (nm)	114	132	140	161	185
C_v (%)	14	10	14	12	15

Figure 3. (a) TEM image and photograph of colloidal suspensions of Si NSs. (b) High-resolution TEM image of a Si NS. (c) Raman scattering spectra of a Si NS (red curve) and a Si wafer (gray

curve). (d) Measured (red curve) and calculated (gray dashed curve) scattering spectra of a single Si NS with the diameter of 156 nm. (e) Photographs of Si NS suspensions after a size-separation process. The average diameter (d_{ave}) and the coefficients of variation of the size distribution (C_v) defined by the standard deviation divided by d_{ave} are shown below the photos. (f) Extinction spectra of Si NS suspensions with 114 to 185 nm in diameters. (g) SEM image of a Si NS monolayer prepared by the LB method.

Figure 4a shows photographs of Si NS monolayers formed on SiO_2/Si substrates. The average diameter of Si NSs is changed from 114 to 185 nm (horizontal axis), and the SiO_2 thickness is changed from 0 to 200 nm (vertical axis). The background is a black paper, and the samples are illuminated from the top by a white LED. We can see the change of the Mie scattering color depending on not only the diameter, but also the spacer thickness. For example, in the monolayer of 161 nm-diameter Si NSs, the color changes from green to yellow and then returns to greenish as the SiO_2 thickness increases. Figures 4b shows the diffuse reflectance spectra of monolayers of 161 nm-diameter Si NSs on different SiO_2 thickness substrates. It is important to note that if Si NSs in the monolayers have exactly the same size and are perfectly aligned, the reflectance should be predominantly the specular reflectance. The appearance of small diffuse reflectance (~10 %) in Figure 4b indicates the existence of non-uniformities and irregularities in the structure.[14] This is consistent with the SEM image in Figure 3d. In the diffuse reflectance spectra, at t_s = 0, *i.e.* no spacer, a peak appears at ~550 nm. With increasing t_s, an additional peak appears at ~670 nm and becomes dominant at t_s = 108 nm. Further increase of the thickness to 200 nm results in the decrease of the ~670 nm peak and reappearance of the ~550 nm peak. This behavior is very similar

to that shown in Figure 1 for a single Si NS on a SiO_2/Si substrate. From this spacer thickness dependence, the ~550 nm and ~670 nm peaks are assigned to the ED and MD modes, respectively.

Figure 4c shows the specular reflectance spectra of the same samples. The intensity of the specular reflectance is larger than that of the diffuse reflectance and has more pronounced features. In the figure, the specular reflectance spectrum of a Si NS monolayer formed on a SiO_2 substrate (grey dashed curve, "w/o Si mirror") is also shown. The ~570 nm peak of the Si NS monolayer on a SiO_2 substrate is a Mie mode, since no Fabry–Pérot mode exists in the structure. In Si NS monolayers on SiO_2/Si substrates, the ~570 nm Mie mode peak is modulated by the SiO_2 film thickness; it shifts from 550 to 700 nm by coupling with the Fabry–Pérot mode, and at t_s = 200 nm, it splits into two peaks.

Figure 4d shows the total reflectance spectra obtained by adding the diffuse and specular reflectance spectra. The total reflectance spectra of monolayers of different sizes Si NSs are shown in Supporting Information (Figure S3). Since the specular reflectance is much stronger than the diffuse reflectance, the total reflectance is very similar to the specular one. Figure 4e (blue dots) shows the reflectance peak wavelengths around 500-700 nm as a function of the spacer thickness. The peak shifts to the longer wavelength with increasing SiO_2 thickness and it splits into two peaks when t_s = 200 nm. This is the reason that the color changes from greenish to yellowish, and then returns to greenish with increasing spacer thickness in Figure 4a. In Figure 4e, the peak wavelengths obtained from calculated reflectance spectra in Figure 2b are also shown by red dots. We can see overall agreement in the experiments and the calculations. Therefore, the color change observed in Figure 4a is due to the coupling of the Mie mode of Si NS monolayers with the Fabry–Pérot cavity mode. Although the observed peak wavelengths agree fairly well with the calculated

ones, the reflectance values (40-45%) are smaller than the calculated ones (~80%). This is due to irregular alignment of NSs and the finite size distributions.

The structural color in Figure 4 shows viewing angle dependence because Fabry–Pérot interference is angle dependence. However, as can be seen in Supporting Information (Figure S7), the angle dependence is small. This is because of non-iridescent structural color of Si NS monolayers,[28] Finally, the structural color is stable in ambient for a long period (see Figure S6 in Supporting Information). This is because native-oxidation of Si surface stops around ~2 nm at room temperature.

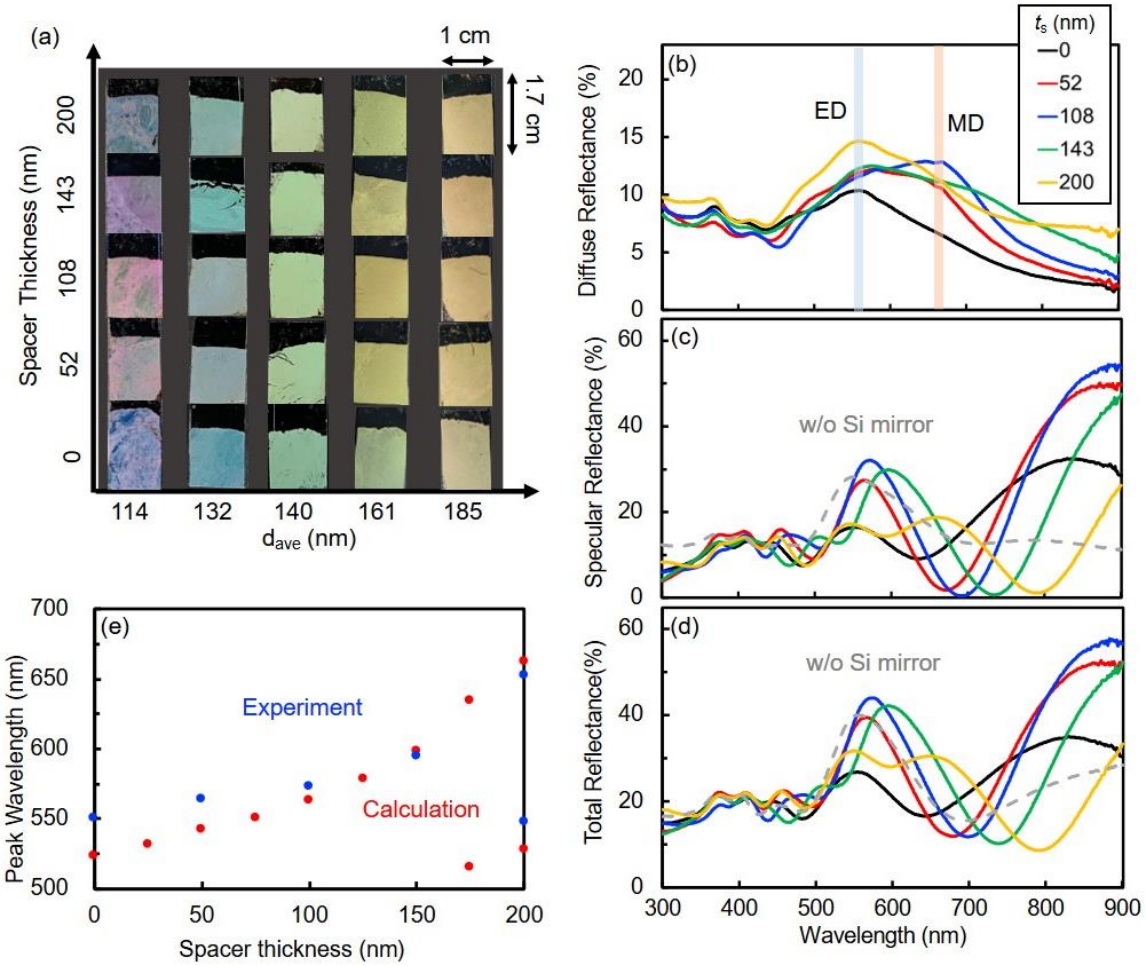

Figure 4. (a) Photographs of Si NS monolayers on SiO_2/Si substrates as functions of Si NS average diameter (d_{ave}) and SiO_2 film thickness (t_s). (b) Diffuse, (c) specular, and (d) total reflectance spectra of Si NS monolayers on SiO_2/Si substrates (d_{ave} = 161 nm). The SiO_2 film thickness is varied from 0 to 200 nm. (e) Reflectance peak wavelengths in a 500-700 nm range of Si NS monolayers (d_{ave} = 161 nm) on SiO_2/Si substrates as a function of SiO_2 film thickness (t_s = 0 - 200 nm).

3. Conclusion

We studied the effect of coupling between Mie modes of Si NS monolayers and a Fabry–Pérot cavity mode on the structural color. Numerical simulations revealed that the reflectance spectra are modified by the coupling and the color changes depending on the cavity length. We fabricated Si NS monolayers on oxidized Si wafers by the LB method. In this structure, the SiO_2 film works as a Fabry–Pérot cavity. By changing the cavity length by the SiO_2 film thickness, we showed that the Mie scattering color of Si NS monolayers is modified, and the color change agrees well with the theoretical prediction. The results will be used, for example, for the development of a colorimetric humidity sensor composed of a Si NS monolayer and a Fabry–Pérot cavity made from a humidity-responsive hydrogel film.[36]

4. Experimental Section

Preparation of Si NS suspension: Si NSs were prepared by thermal disproportionation reaction of silicon monoxide (SiO) lumps.[21,22,28,42] SiO lumps (several mm in size) (Wako, 99 %) were annealed at 1500-1550 ºC in an N_2 gas atmosphere for 30 minutes to grow crystalline Si NSs in SiO_2 matrices. Si NSs were liberated from SiO_2 matrices by etching in hydrofluoric acid (HF)

solution (46 wt.%) for 1 h. Liberated Si NSs were transferred to methanol by the following process. Methanol was added to the HF solution of Si NSs, and the mixture solution was centrifugated for 1 min to precipitate Si NSs. After removing the supernatant liquid, methanol was added to the tube and Si NSs were redispersed.[18] The centrifugation and the solution exchange were repeated several times until the pH of the solution became 4-6. Finally, Si NSs were subject to sonification in methanol with an ultrasonic homogenizer (Violamo SONIVSTAR 85).

Size Separation of Si NSs: Si NSs were separated by size using a sucrose density gradient centrifugation method. A sucrose density gradient solution was prepared by carefully adding 2.2 ml sucrose solutions at six different concentrations (55-42.5 wt.%, 2.5 wt.% increments) to a 15 ml centrifugal tube in order. Methanol solution of Si NSs (1.8 ml) was added to the top of the tube, and the tube was subject to centrifugation at 5500 rpm for 55-60 min to form layers of size-separated Si NSs. The layers were retrieved 1 ml at a time from the top and transferred to different tubes. The solutions of size-separated Si NSs were washed with water several times to remove sucrose and transferred to methanol.

Fabrication of Si NS monolayer on SiO_2/Si substrate: Si NS monolayers were fabricated by the LB method. First, Si NS surface was etched in HF solution (5 wt.%) for 2 min to remove the native oxide and to make the surface hydrophobic, and then they were transferred to butanol. The butanol solution of Si NSs was slowly dropped onto the surface of water in a petri dish to form the monolayer at the air/water interface. Finally, the monolayer was transferred to a SiO_2/Si substrate (1.7 cm×1.0 cm) prepared by oxidation of a Si wafer (1100 °C, 0 - 200 min).

Optical characterization: Extinction spectra of Si NS suspensions were measured using a standard double-beam spectrophotometer (UV-3101PC, Shimadzu). From the spectra, average diameter (d_{ave}) and the coefficients of variation of the size distribution (C_v) defined by the standard deviation divided by d_{ave} were estimated using the method reported in our previous work.[41] Specular reflectance spectra were measured by the same spectrophotometer with the reflection configuration. The incident and detection angles are 5°. The diffuse reflectance spectra were measured by a spectrophotometer equipped with an integrating sphere (Spectrapro3700, Shimadzu). Incident light was unpolarized in both measurements.

Numerical Simulation: The backscattering spectra of single Si NS and reflectance spectra of Si NS monolayers on SiO_2/Si substrates were calculated using commercial software (Lumerical, Ansys) based on the finite-difference time-domain (FDTD) method. For the calculation of backscattering spectra of a single Si NS, a total-field scattering-field (TFSF) source and perfectly matched layers (PML) for *x*, *y* and *z* directions were used. The collection angle of scattered light was approximately 53^o (NA = 0.8). For the calculation of reflection spectra of Si NS monolayers, the periodic boundary condition was used for the *x* and *y* directions, and the perfectly matched layer (PML) boundary was used for the z-direction. The complex refractive index of Si is taken from a literature.[43]

ASSOCIATED CONTENT

Supporting Information. Additional calculated scattering and reflection spectra, experimental results on substrates and angle dependent reflection spectra (PDF)

Corresponding Author

*sugimoto@eedept.kobe-u.ac.jp

ACKNOWLEDGMENT

This work was supported by JSPS KAKENHI grant numbers, 18KK0141, 21H01748, 22K18949 and 21H01782.

References

(1) Ghiradella, H. Light and Color on the Wing: Structural Colors in Butterflies and Moths. *Appl. Opt.* **1991**, *30* (24), 3492. https://doi.org/10.1364/AO.30.003492.
(2) Ghiradella, H. The Wings and Cuticles of Insects Have Much to Teach Us in Areas Such as Thin Films, Lattice Structures, Iridescence,.
(3) Holsteen, A. L.; Raza, S.; Fan, P.; Kik, P. G.; Brongersma, M. L. Purcell Effect for Active Tuning of Light Scattering from Semiconductor Optical Antennas. *Science* **2017**, *358* (6369), 1407–1410. https://doi.org/10.1126/science.aao5371.
(4) Baek, K.; Kim, Y.; Mohd-Noor, S.; Hyun, J. K. Mie Resonant Structural Colors. *ACS Appl. Mater. Interfaces* **2020**, *12* (5), 5300–5318. https://doi.org/10.1021/acsami.9b16683.
(5) Tan, S. J.; Zhang, L.; Zhu, D.; Goh, X. M.; Wang, Y. M.; Kumar, K.; Qiu, C.-W.; Yang, J. K. W. Plasmonic Color Palettes for Photorealistic Printing with Aluminum Nanostructures. *Nano Lett.* **2014**, *14* (7), 4023–4029. https://doi.org/10.1021/nl501460x.
(6) Roberts, A. S.; Pors, A.; Albrektsen, O.; Bozhevolnyi, S. I. Subwavelength Plasmonic Color Printing Protected for Ambient Use. *Nano Lett.* **2014**, *14* (2), 783–787. https://doi.org/10.1021/nl404129n.
(7) Olson, J.; Manjavacas, A.; Liu, L.; Chang, W.-S.; Foerster, B.; King, N. S.; Knight, M. W.; Nordlander, P.; Halas, N. J.; Link, S. Vivid, Full-Color Aluminum Plasmonic Pixels. *Proc. Natl. Acad. Sci.* **2014**, *111* (40), 14348–14353. https://doi.org/10.1073/pnas.1415970111.
(8) Li, Z.; Clark, A. W.; Cooper, J. M. Dual Color Plasmonic Pixels Create a Polarization Controlled Nano Color Palette. *ACS Nano* **2016**, *10* (1), 492–498. https://doi.org/10.1021/acsnano.5b05411.
(9) Park, C.-S.; Koirala, I.; Gao, S.; Shrestha, V. R.; Lee, S.-S.; Choi, D.-Y. Structural Color Filters Based on an All-Dielectric Metasurface Exploiting Silicon-Rich Silicon Nitride Nanodisks. *Opt. Express* **2019**, *27* (2), 667. https://doi.org/10.1364/OE.27.000667.
(10) Dong, Z.; Ho, J.; Yu, Y. F.; Fu, Y. H.; Paniagua-Dominguez, R.; Wang, S.; Kuznetsov, A. I.; Yang, J. K. W. Printing Beyond sRGB Color Gamut by Mimicking Silicon Nanostructures in Free-Space. *Nano Lett.* **2017**, *17* (12), 7620–7628. https://doi.org/10.1021/acs.nanolett.7b03613.
(11) Kuznetsov, A. I.; Miroshnichenko, A. E.; Fu, Y. H.; Zhang, J.; Luk'yanchuk, B. Magnetic Light. *Sci. Rep.* **2012**, *2* (1), 492. https://doi.org/10.1038/srep00492.

(12) Fu, Y. H.; Kuznetsov, A. I.; Miroshnichenko, A. E.; Yu, Y. F.; Luk'yanchuk, B. Directional Visible Light Scattering by Silicon Nanoparticles. *Nat. Commun.* **2013**, *4* (1), 1527. https://doi.org/10.1038/ncomms2538.
(13) Cao, L.; Fan, P.; Barnard, E. S.; Brown, A. M.; Brongersma, M. L. Tuning the Color of Silicon Nanostructures. *Nano Lett.* **2010**, *10* (7), 2649–2654. https://doi.org/10.1021/nl1013794.
(14) Yao, X.; Hong, X.; Liu, Y. Visible Mie Resonances in Dielectric Hollow Spheres: Principle, Regulation, and Applications. *Responsive Mater.* **2023**, *1* (2), e20230019. https://doi.org/10.1002/rpm.20230019.
(15) Jahani, S.; Jacob, Z. All-Dielectric Metamaterials. *Nat. Nanotechnol.* **2016**, *11* (1), 23–36. https://doi.org/10.1038/nnano.2015.304.
(16) Zhao, Q.; Zhou, J.; Zhang, F.; Lippens, D. Mie Resonance-Based Dielectric Metamaterials. *Mater. Today* **2009**, *12* (12), 60–69. https://doi.org/10.1016/S1369-7021(09)70318-9.
(17) Kuznetsov, A.; Miroshnichenko, A.; Brongersma, M.; Kivshar, Y.; Luk'yanchuk, B. Optically Resonant Dielectric Nanostructures. *Science* **2016**, *354*, null. https://doi.org/10.1126/science.aag2472.
(18) Sugimoto, H.; Okazaki, T.; Fujii, M. Mie Resonator Color Inks of Monodispersed and Perfectly Spherical Crystalline Silicon Nanoparticles. *Adv. Opt. Mater.* **2020**, *8* (12), 2000033. https://doi.org/10.1002/adom.202000033.
(19) Nagasaki, Y.; Hotta, I.; Suzuki, M.; Takahara, J. Metal-Masked Mie-Resonant Full-Color Printing for Achieving Free-Space Resolution Limit. *ACS Photonics* **2018**, *5* (9), 3849–3855. https://doi.org/10.1021/acsphotonics.8b00895.
(20) Yang, W.; Xiao, S.; Song, Q.; Liu, Y.; Wu, Y.; Wang, S.; Yu, J.; Han, J.; Tsai, D.-P. All-Dielectric Metasurface for High-Performance Structural Color. *Nat. Commun.* **2020**, *11* (1), 1864. https://doi.org/10.1038/s41467-020-15773-0.
(21) Okazaki, T.; Sugimoto, H.; Hinamoto, T.; Fujii, M. Color Toning of Mie Resonant Silicon Nanoparticle Color Inks. *ACS Appl. Mater. Interfaces* **2021**, *13* (11), 13613–13619. https://doi.org/10.1021/acsami.1c01692.
(22) Sugimoto, H.; Fujii, M. Colloidal Mie Resonant Silicon Nanoparticles. *Nanotechnology* **2021**, *32* (45), 452001. https://doi.org/10.1088/1361-6528/ac1a44.
(23) Lee, T.; Kim, J.; Koirala, I.; Yang, Y.; Badloe, T.; Jang, J.; Rho, J. Nearly Perfect Transmissive Subtractive Coloration through the Spectral Amplification of Mie Scattering and Lattice Resonance. *ACS Appl. Mater. Interfaces* **2021**, *13* (22), 26299–26307. https://doi.org/10.1021/acsami.1c03427.
(24) Li, L.; Niu, J.; Shang, X.; Chen, S.; Lu, C.; Zhang, Y.; Shi, L. Bright Field Structural Colors in Silicon-on-Insulator Nanostructures. *ACS Appl. Mater. Interfaces* **2021**, *13* (3), 4364–4373. https://doi.org/10.1021/acsami.0c19126.
(25) Nagasaki, Y.; Suzuki, M.; Takahara, J. All-Dielectric Dual-Color Pixel with Subwavelength Resolution. *Nano Lett.* **2017**, *17* (12), 7500–7506. https://doi.org/10.1021/acs.nanolett.7b03421.
(26) Proust, J.; Bedu, F.; Gallas, B.; Ozerov, I.; Bonod, N. All-Dielectric Colored Metasurfaces with Silicon Mie Resonators. *ACS Nano* **2016**, *10* (8), 7761–7767. https://doi.org/10.1021/acsnano.6b03207.
(27) Jang, J.; Badloe, T.; Yang, Y.; Lee, T.; Mun, J.; Rho, J. Spectral Modulation through the Hybridization of Mie-Scatterers and Quasi-Guided Mode Resonances: Realizing Full and Gradients of Structural Color. *ACS Nano* **2020**, *14* (11), 15317–15326. https://doi.org/10.1021/acsnano.0c05656.

(28) Tanaka, H.; Hotta, S.; Hinamoto, T.; Sugimoto, H.; Fujii, M. Monolayer of Mie-Resonant Silicon Nanospheres for Structural Coloration. *ACS Appl. Nano Mater.* **2024**, acsanm.3c04689. https://doi.org/10.1021/acsanm.3c04689.
(29) Zou, C.; Komar, A.; Fasold, S.; Bohn, J.; Muravsky, A.; Murauski, A.; Pertsch, T.; Neshev, D.; Staude, I. Electrically Tunable Transparent Displays for Visible Light Based on Dielectric Metasurfaces. *ACS Photonics* **2019**, *null*, null. https://doi.org/10.1021/ACSPHOTONICS.9B00301.
(30) Komar, A.; Fang, Z.; Bohn, J.; Sautter, J.; Decker, M.; Miroshnichenko, A.; Pertsch, T.; Brener, I.; Kivshar, Y.; Staude, I.; Neshev, D. Electrically Tunable All-Dielectric Optical Metasurfaces Based on Liquid Crystals. *Appl. Phys. Lett.* **2017**, *110*, 071109. https://doi.org/10.1063/1.4976504.
(31) Holsteen, A. L.; Cihan, A. F.; Brongersma, M. L. Temporal Color Mixing and Dynamic Beam Shaping with Silicon Metasurfaces. *Science* **2019**, *365* (6450), 257–260. https://doi.org/10.1126/science.aax5961.
(32) Gutruf, P.; Zou, C.; Withayachumnankul, W.; Bhaskaran, M.; Sriram, S.; Fumeaux, C. Mechanically Tunable Dielectric Resonator Metasurfaces at Visible Frequencies. *ACS Nano* **2016**, *10 1*, 133–141. https://doi.org/10.1021/acsnano.5b05954.
(33) Ee, H.-S.; Agarwal, R. Tunable Metasurface and Flat Optical Zoom Lens on a Stretchable Substrate. *Nano Lett.* **2016**, *16* (4), 2818–2823. https://doi.org/10.1021/acs.nanolett.6b00618.
(34) Ge, D.; Lee, E.; Yang, L.; Cho, Y.; Li, M.; Gianola, D. S.; Yang, S. A Robust Smart Window: Reversibly Switching from High Transparency to Angle-Independent Structural Color Display. *Adv. Mater.* **2015**, *27* (15), 2489–2495. https://doi.org/10.1002/adma.201500281.
(35) Mohd-Noor, S.; Jang, H.; Baek, K.; Pei, Y.-R.; Alam, A.-M.; Kim, Y. H.; Kim, I. S.; Choy, J.-H.; Hyun, J. K. Ultrafast Humidity-Responsive Structural Colors from Disordered Nanoporous Titania Microspheres. *J. Mater. Chem. A* **2019**, *7* (17), 10561–10571. https://doi.org/10.1039/C9TA01394F.
(36) Jung, C.; Kim, S.-J.; Jang, J.; Ko, J. H.; Kim, D.; Ko, B.; Song, Y. M.; Hong, S.-H.; Rho, J. Disordered-Nanoparticle–Based Etalon for Ultrafast Humidity-Responsive Colorimetric Sensors and Anti-Counterfeiting Displays. *Sci. Adv.* **2022**, *8* (10), eabm8598. https://doi.org/10.1126/sciadv.abm8598.
(37) Lather, J.; Bhatt, P.; Thomas, A.; Ebbesen, T. W.; George, J. Cavity Catalysis by Cooperative Vibrational Strong Coupling of Reactant and Solvent Molecules. *Angew. Chem. Int. Ed.* **2019**, *58* (31), 10635–10638. https://doi.org/10.1002/anie.201905407.
(38) Osgood, R. M.; Ait-El-Aoud, Y.; Bullion, K.; Dinneen, S.; Kingsborough, R.; Rothschild, M.; Kooi, S. Fabry-Perot Interference Pattern Scattered by a Sub-Monolayer Array of Nanoparticles. *Mater. Res. Express* **2022**, *9* (1), 016202. https://doi.org/10.1088/2053-1591/ac487c.
(39) Kim, T.; Lee, J.; Yu, E.; Lee, S.; Woo, H.; Kwak, J.; Chung, S.; Choi, I.; Ryu, Y. Fabry–Perot Cavity Control for Tunable Raman Scattering. *Small* **2023**, *19* (29), 2207003. https://doi.org/10.1002/smll.202207003.
(40) Hinamoto, T.; Fujii, M. MENP: An Open-Source MATLAB Implementation of Multipole Expansion for Nanophotonics. *OSA Contin.* **2021**, *4* (5), 1640. https://doi.org/10.1364/OSAC.425189.
(41) Negoro, H.; Sugimoto, H.; Fujii, M. Helicity-Preserving Optical Metafluids. *Nano Lett.* **2023**, *23* (11), 5101–5107. https://doi.org/10.1021/acs.nanolett.3c01026.

(42) Sugimoto, H.; Okazaki, T.; Fujii, M. Mie Resonator Color Inks of Monodispersed and Perfectly Spherical Crystalline Silicon Nanoparticles. *Adv. Opt. Mater.* **2020**, *8* (12), 2000033. https://doi.org/10.1002/adom.202000033.
(43) Palik, E. D. *Handbook of Optical Constants of Solids*; Academic press, 1998; Vol. 3、pp.519.

TOC

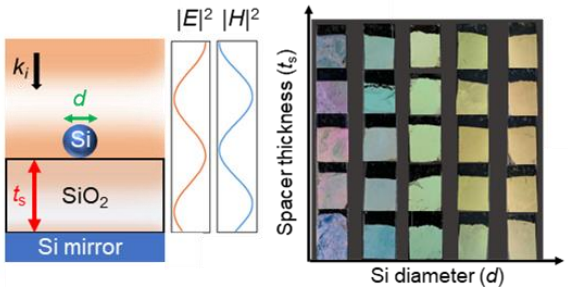
$|E|^2$ $|H|^2$
k_i
d
Si
t_s
SiO_2
Si mirror
Spacer thickness (t_s)
Si diameter (d)